J Nanopart Res (2014) 16:2571
DOI 10.1007/s11051-014-2571-3

RESEARCH PAPER

Green synthesis of Au nanoparticles using potato extract: stability and growth mechanism

D. N. Castillo-López · U. Pal

Received: 2 January 2014 / Accepted: 15 July 2014 / Published online: 1 August 2014

Abstract We report on the synthesis of spherical, well-dispersed colloidal gold nanoparticles of 17.5–23.5 nm average sizes in water using potato extract (PE) both as reducing and stabilizing agent. The effects of PE content and the pH value of the reaction mixture have been studied. Formation and growth dynamics of the Au nanoparticles in the colloids were studied using transmission electron microscopy and UV-Vis optical absorption spectroscopy techniques. While the reductor content and, hence, the nucleation and growth rates of the nanoparticles could be controlled by controlling the PE content in the reaction solution, the stability of the nanoparticles depended strongly on the pH of the reaction mixture. The mechanisms of Au ion reduction and stabilization of Au nanoparticles by potato starch have been discussed. The use of common natural solvent like water and biological reductor like PE in our synthesis process opens up the possibility of synthesizing Au nanoparticles in fully green (environmental friendly) way, and the Au nanoparticles produced in such way should have good biocompatibility.

Keywords Biosynthesis · Potato starch · Gold colloids · Bio-reduction · Bio-capping · Growth mechanism

D. N. Castillo-López · U. Pal (✉)
Instituto de Física, Benemérita Universidad Autónoma de Puebla, Apdo. Postal J-48, Puebla 72570, PUE, Mexico
e-mail: upal@ifuap.buap.mx

Introduction

Synthesis of nanomaterials with controlled size and shape is the fundamental aspect, which defines the utility of these materials in technology. Though a remarkable research effort has been devoted so far to synthesize or fabricate nanomaterials of diverse characteristics, application of these materials in technology depends strongly on their adaptability to the specific system (De et al. 2008; Salata 2004). In fact, controlling these aspects, metal, semiconductor, even dielectric nanostructures could be utilized effectively in the fields of optics, optoelectronics, environment, medicine, and biotechnology (Iskandar 2009; Maurer-Jones et al. 2013; De et al. 2008; Salata 2004). In particular, for applications in bio-nanotechnology, a modern and attractive research area which seeks the intersection between biology and nanotechnology, nanomaterials need to be biocompatible. Considering environmental aspects and adaptability in biotechnology, the methods of nanomaterial synthesis have also been evolved. Several biological methods have been utilized as alternative approaches for the synthesis of inorganic materials, which are environmental friendly, non-toxic or nonhazardous, cheap, and simple (Thakkar et al. 2010). In particular, the synthesis of metallic nanoparticles (NPs) using constituents of biological entities has received a great attention during the last decade, not only due to the remarkable physical and chemical properties inherent to metallic nanoparticles (Schmid 1992) and potential applications in the areas

of optics (Ghosh and Pal 2007; Ricard et al. 1985; Alschinger et al. 2003; Zijlstra and Orrit 2011), electronics (Schmid 1992), catalysis (Ghosh and Pal 2007; Haruta 1997; Lewis 1993; Daniel and Astruc 2004), etc., but also as alternative, environmental friendly approach adaptable for biological (Daniel and Astruc 2004; De et al. 2008; Durán et al. 2007; Salata 2004) and medicinal (Salata 2004; Huang et al. 2007) applications. While a precise control of the shape and size of these nanoparticles is essential for the applications in the former three areas, for the latter two fields (as well in catalysis), apart from their size, the nanoparticles needed to be compatible with biological systems. Since the first work reported on biosynthesis of gold (Au) nanoparticles employing alfalfa by Gardea-Torresdey et al. in 2002, research on the biosynthesis of metallic nanoparticles has been increased many folds, using different parts of plants such as leaves (Shankar et al. 2004; Vilchis-Nestor et al. 2008), bulbs (Parida et al. 2011), rhizomes (Singh et al. 2011; Maheswari et al. 2012), and tubers (Engelbrekt et al. 2004), exploiting the reduction and stabilization potentials of their constituents such as proteins, polysaccharides, and vitamins. For example, biosynthesis of gold (Au) and silver (Ag) nanoparticles of different sizes has been reported using phenolic compounds extracted from *Camellia sinensis* (Vilchis-Nestor et al. 2008), which act both as reducing and stabilizing agent. Ag nanoparticles could be biosynthesized using starch and polyphenols from nopal, *Opuntia ficus,* (Silva-de-Hoyos et al. 2012). Au and Ag nanoparticles could be synthesized using cereal grains like oat (*Avena sativa*) and wheat (*Triticum aestivum*) (Armendariz et al. 2002). Synthesis of Ag and Au nanoparticles using starch as stabilizing agent and β-D glucose as reductor has also been reported (Raveendran et al. 2003; Hussain et al. 2009). Although most of these published works report on the biosynthesis of metallic NPs along with the effects of solution pH, aging time, or the nature of bioreductors like glucose, proteins, amino acids, etc. (Vilchis-Nestor et al. 2008; Silva-de-Hoyos et al. 2012; Bo et al. 2008; Sperling and Parak 2010), none of them discussed the mechanism of reduction and/or stabilization process. In the present article, we report on the synthesis of stable Au nanoparticles with potato extract as unique reducing and stabilizing agent, without pH control of the reaction medium. Tentative mechanisms of Au^{3+} ion reduction and stabilization of the formed Au NPs have been proposed. Unlike the reports published in the literature (Engelbrekt et al. 2004), we demonstrate that potato starch can act as reducing agent for Au^{3+} ions even in acidic media, requiring no external control of the pH of the reaction mixture.

Experimental

Preparation of potato extract

For the synthesis of Au nanoparticles, we used potato (*Solanum tuberosum*) extract as the unique reducing and stabilizing agent, chloroauric acid ($HAuCl_4 \bullet 3H_2O$, Sigma-Aldrich) as the metal precursor, and deionized (DI) water ($\rho > 18.2$ MΩ cm) as dispersing medium. For the preparation of potato extract (PE), a few pieces of peeled potato (50 g) were boiled at 95 °C for 5 min in DI water. After cooling to room temperature, the mixture was filtered using pellon (polyester fabric). Finally, the solution was sterilized using a steel autoclave (PRESTO) at 115 °C and 10 Psi.

Synthesis of Au NPs

Several aqueous solutions with different PE contents were prepared by mixing $(20-x)$ ml of deionized water and x ml of PE ($x = 1.0, 2.0, 3.0$, and 5.0). Then, about 0.5 ml of Au ion solution (5.0 mM) was added to each of the previous solutions. All these solutions were prepared at room temperature (RT), without adjusting their pH, and without agitation. Therefore, all the solutions were of acidic (Table 1) in nature. After adding Au ions, the mixture solutions were kept in dark avoiding their exposure to any external radiation or stray light. The samples were designated according to their PE contents as 1PE, 2PE, 3PE, and 5PE. A spontaneous and gradual color change could be noticed after the addition of Au ions in the solutions, indicating the reduction of metal ions.

Characterization of Au NPs

Room temperature UV-Vis absorption spectra of the colloidal solutions were recorded at different intervals in a Shimadzu UV3101PC dual beam spectrophotometer using a square quartz cell of 1.0 cm optical path

Table 1 pH of the reaction mixtures before and after the addition of Au ion solution

Samples	1PE	2PE	3PE	5PE
pH (before adding gold ions)	6.33 ± 0.02	6.28 ± 0.02	6.20 ± 0.03	6.15 ± 0.02
pH (after adding gold ions)	3.86 ± 0.03	4.28 ± 0.02	4.57 ± 0.02	4.97 ± 0.04

length. For microscopic observation of the nanoparticles, a Jeol JEM ARM 200F transmission electron microscope (TEM) operating at 200 kV was utilized. The samples for TEM observation were prepared by dispersing a drop of colloidal suspension on carbon-coated copper grid, followed by drying at room temperature.

Results and discussion

Biosynthesis of Au NPs

In this section, we will discuss the mechanisms behind the formation and stabilization of gold nanoparticles while using potato extract both as reductor and as stabilizer without pH adjustment of the reaction solution (acidic medium).

PE as biological reductor for Au ions

Potato constitutes about 79 % water, 19 % starch, and rest 2 % proteins, lipids, and acids; wherein, the starch is composed of 20 % amylose [lineal chain made of α(1,4) D-glucose units] and 80 % amylopectin [chain of α(1,4) D-glucose branched with other D-glucose units through α(1,6) bonds]. These percentages can vary depending upon tuber species. During potato extract preparation, when the pieces of potato are boiled with DI water, the starch grains swell, and both amylose and amylopectin leach out from the granules, though the process is slower for the latter. At the subjected temperature of boiling (95 °C), a very small fraction of both amylose and amylopectin break down into smaller chains of a few glucose units due to the breaking of glycosidic bonds, exposing more aldehyde groups, as reported by several researchers (Kardos and Luche 2001; Sriburi and Hill 2000; Liu et al. 2010). The chain-breaking process continues even at greater rate during sterilization of the solutions (at 110 °C and 10 Psi), exposing a greater number of aldehyde groups, which act as reducing agent for Au ions.

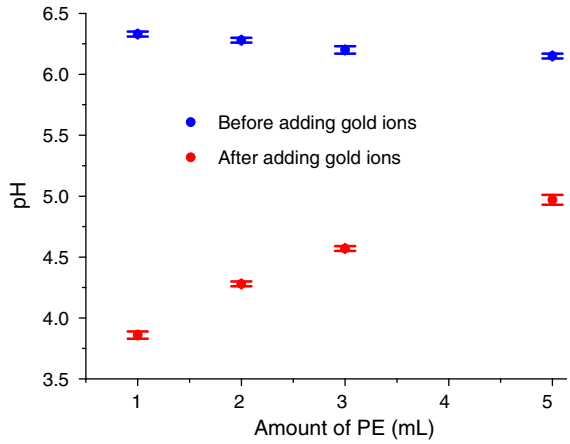

Fig. 1 Variation of pH of the reaction mixture with the variation of PE content. The pHs of used water and PE were 6.49 and 6.1, respectively

An important parameter to be considered in our synthesis is the pH of the reaction solution, since all the Au nanoparticles were prepared without pH adjustment. The pH of the reaction solutions was measured before pouring gold ions and after dissolving them in the solutions. The pH values of the *x*PE solutions ($x = 1.0$, 2.0, 3.0, and 5.0) were compared with pH values of the solutions after the addition of Au ion solution. From the plot presented in Fig. 1, we can observe that by increasing the concentration of PE (in water), solution acidity increases (e.g. $pH_{1PE} > pH_{5PE}$), and by the addition of Au ions, the solutions containing lower contents of PE become more acidic (e.g. $pH_{1PE} < pH_{5PE}$). The reduction of solution pH value with the increase of PE content is expected as the pH of the used potato extract was of about six. As the gold chloride is highly acidic in nature, by pouring gold ions in the reaction mixture, the concentration of protons (H^+) increases, which breaks down some of the glycosidic bonds of amylose and amylopectin (present in the solution) through hydrolysis as shown in Fig. 2 (Kupiainen 2012), producing more glucose units and causing a decrease of H^+ ion concentration

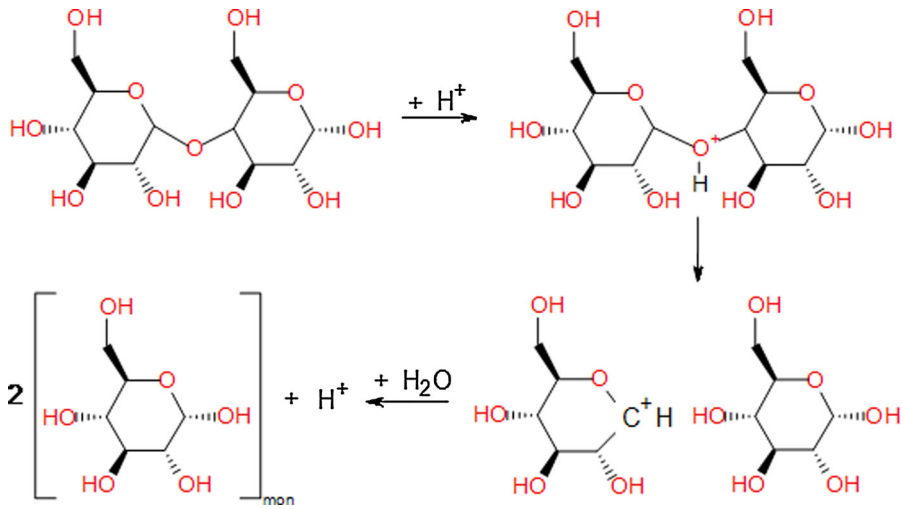

Fig. 2 Schematic representation of hydrolysis process of D-glucose chain in acidic medium

in the reaction solution. The presence of PE in higher amount in the reaction mixture produces glucose units in higher numbers, causing a greater diminution of solution acidity.

Reduction of Au ions

D-glucose ($C_6H_{12}O_6$) is frequently referred as aldohexose as it constitutes of six carbon atoms (hexose) and an aldehyde group (–CHO) at one end. It is the latter that gives D-glucose the reductor character. The reducing behavior of aldehyde group has been exploited through the conventional *Tollens test*, in which silver ions are reduced (Benet et al. 2011). Reduction of gold ions by glucose to produce Au NPs in acidic medium has been reported without providing the details of reactions (Liu et al. 2006).

In Fig. 3, different steps of the redox reactions of gold ions with D-glucose are presented schematically. On addition of Au solution in the reaction mixture, first the Au^{3+} ions get attached to the oxygen of the aldehyde groups because of their free electrons, and get reduced to Au^{2+} ions. The process is followed by the nucleophilic substitution, where a hydroxyl radical (OH^-) gets attached to the sixth carbon of the glucose chain. Due to the instability of this carbon in the presence of OH^- ion, the hydrogen atom gets unlinked from the carbon, and transfers its electron to Au^{2+} ion, reducing it to Au^{1+}.The oxygen of the carbonyl group recovers its double bond. Thus D-glucose is converted to gluconic acid (eq. 1). Reduction of Au^{1+} to atomic gold (Au^0) is also carried out through a similar reaction (eq. 2).

PE as stabilizing agent for Au NPs

Regarding the nanoparticle stabilization, capping of Fe nanoparticles through electrostatic attraction between the hydroxyl group of gluconic acid and the nanoparticle surface has already been reported (Sui et al. 2012). There also exist reports on the stabilization of Au and Ag nanoparticles through hydroxyl groups of the starch molecules (Hussain et al. 2009; Sperling and Parak 2010; Liu et al. 2006).

As we discussed earlier, the PE solution used for the reduction of gold ions containing D-glucose units also contained short-chained amylose and amylopectin. Both amylose and amylopectin chains have a D-glucose unit in one of their ends where no anomeric carbon is involved to form glycosidic bond. This end is known as reducing end. The reducing end gets oxidized in the presence of Au ions, transforming the terminal D-glucose unit to gluconic acid (Figs. 3, 4a). The negative charge on the oxygen of the hydroxyl group of gluconic acid interacts with the surface positive charge of Au NPs via electrostatic interaction, causing their bonding. On the other hand, hydroxyl groups of the amylopectin chains, especially the external hydroxyl groups of amylose helical chains get bonded with the surface of Au nanoparticles

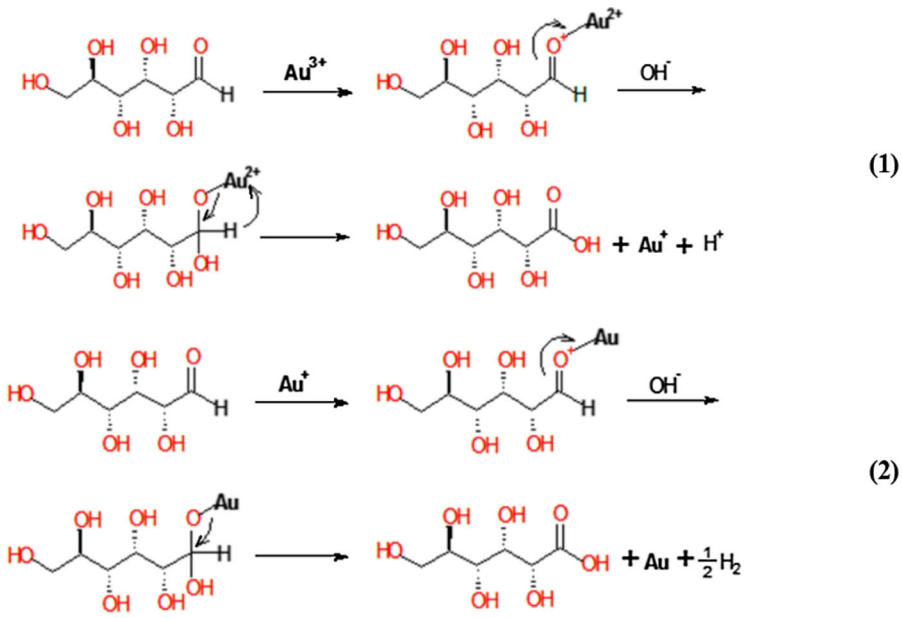

Fig. 3 Schematic presentation of the proposed Au ion reduction reactions by PE

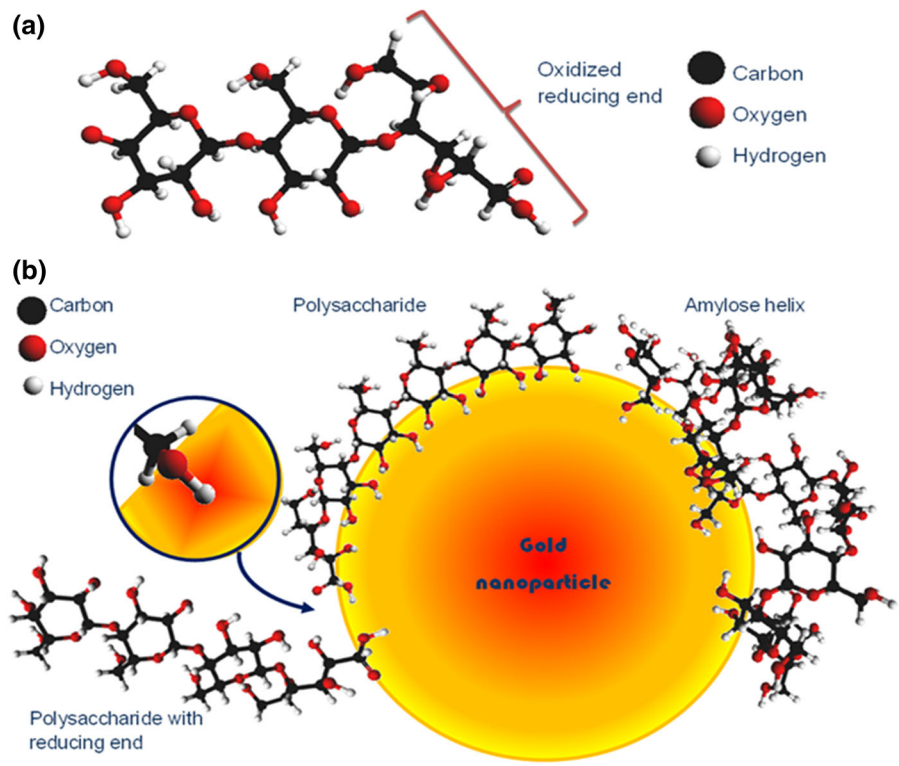

Fig. 4 **a** A polysaccharide chain with oxidized reducing end, and **b** a schematic illustration of polysaccharide adsorption process at the surface of gold nanoparticle bonded through (OH^-) groups

through electrostatic interaction (Hussain et al. 2009). We believe both these capping mechanisms are responsible for the stabilization of Au NPs (Fig. 4b) in our synthesis.

As mentioned earlier, the pH of our reaction mixture varied with PE content, mainly due to the breaking of amylose and amylopectin chains. The polysaccharide chains remain partially hydrolyzed

under the reaction conditions (temperature and pH) we utilized. On increasing the PE content in the reaction solution of a fixed pH value, there is an increase in the amount of partially broken chains (with oxidized reducing end due to the reduction of Au ions), producing a greater amount of stabilizing agent. However, as we can see from the TEM images of our samples (presented later), the dispersion of nanoparticle size gets compromised with the increase of PE content in the reaction solution due to the increase of reducing agent and, hence, a higher nucleation rate of Au particles.

While the growth and size control of the Au NPs were controlled by the electrostatic interaction between the NP surface and the glucose or polysaccharide molecules, the aggregation of the formed NPs is controlled by the steric interaction of the polysaccharides adsorbed on the NP surface. Therefore, it is important to form a dense layer of these polysaccharides around the nanoparticles for stabilization.

Optical absorption study of Au colloids

The growth dynamics of Au nanoparticles in the reaction mixtures was studied by recording the absorption spectra of the reaction solutions at different intervals after the addition of Au ions in them (Fig. 5). The absorption spectra of colloidal samples reveal a peak in between 536 and 551 nm (Figs. 5, 6), associated to the surface plasmon resonance (SPR) of Au nanoparticles (Ghosh and Pal 2007; De et al. 2008; Jain et al. 2006; Eustis and El-Sayed 2006). Appearance of SRP band in the absorption spectra could be noted after about 7 h of preparation of the samples. The SRP band in all the colloidal samples grows with time. The amount of PE in the reaction mixture was found to control both the position and intensity of the SPR band in more severe ways than the reaction time. On increasing the concentration of PE, the SPR band appeared toward higher wavelengths (Fig. 6). We attribute this red shift mainly to an increase of refractive index (n) of the medium by the increase of PE content ($n_{PE} > n_{water}$), as the position of SPR band depends on the refractive index of colloidal media (Ghosh and Pal 2007; Eustis and El-Sayed 2006; Mock et al. 2003; Kelly et al. 2003), while the possibility of red shift of the SPR band due to the formation of bigger NPs in the reaction solution cannot be discarded. As can be seen in Fig. 5, the shape of the SPR band becomes slightly wider by increasing the concentration of PE, which is associated to greater dispersion of particle size, as supported by their TEM observations (discussed later).

The SPR band for the 1PE sample appeared at about 536 nm on the first day, and gradually shifted to about 534 nm after 3 days of preparation. A less intense band appeared as the shoulder of the main absorption band at higher wavelength side (at about 620 nm) after 10 days of preparation of the sample, which we will discuss later. For the 2PE sample, the SPR band appeared at 540 nm on the first day and shifted to 534 nm (blue shift) after 10 days of preparation. The same happened with the 3PE and 5PE samples, where the SPR band appeared at about 535 and 536 nm, respectively, after 10 days of preparation. The small blue shift of the SPR band with time for all the four samples is due to the gradual change in composition of the reaction mixtures occurred due to the continuous reduction of glucose and capping process of the formed gold nanoparticles. Although a blue shift of SPR band has been observed for Au colloids prepared by laser ablation of Au ion solutions and attributed to the size reduction of the nanoparticles due to extended laser irradiation (Courrol et al. 2007; Herbani et al. 2010), we discard this possibility in the present case, as no external energy was supplied in our synthesis (the reaction mixtures were kept in dark and at room temperature). After about 12 days of preparation, the position of the SPR band stabilized for all the samples until about 20 days, and thereafter it moved toward higher wavelengths. While the change in SPR peak position (blue shift) during the first 12 days could be associated to the gradual change occurred in the reaction mixture composition, the change after 20 days (red shift of SPR band) could be associated to the aggregation process of Au nanoparticles.

TEM and HRTEM study of Au NPs

Figure 7 shows typical TEM images of the Au nanoparticles formed in each sample along with their size distribution histograms. The size distribution histogram of the 1PE sample (Fig. 7a) obtained from its TEM images recorded after 1 day of reaction shows the formation of well-dispersed Au nanoparticles of sizes in between 2 and 25 nm, with an average size of 3.4 ± 0.6 nm. The size distribution histogram of the nanoparticles of the same sample after 10 days of

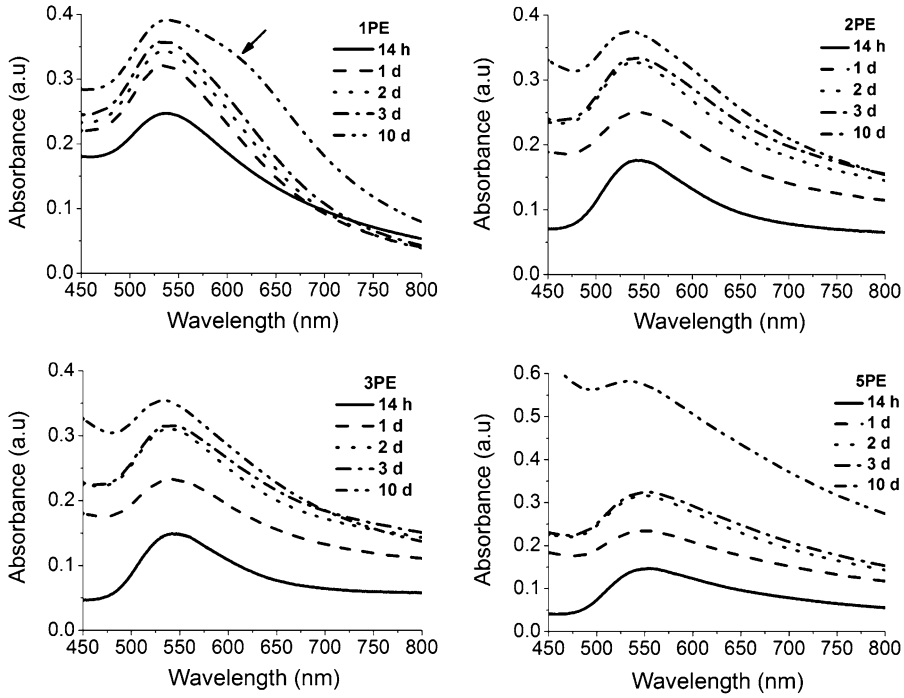

Fig. 5 Absorption spectra of 1PE, 2PE, 3PE, and 5PE samples recorded at different intervals (after 14 h, 1, 2, 3, and 10 days of their preparation)

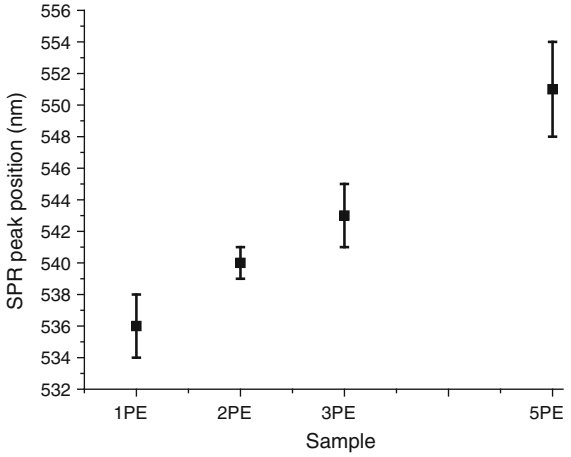

Fig. 6 Variation of SPR peak position with PE content in the reaction mixtures. The measurements were performed after 14 h of preparation of the reaction solutions (after the addition of Au ion solution)

reaction revealed a bimodal distribution (Fig. 7b), with two groups of particles with average sizes of 5.7 ± 0.9 (see the inset of Fig. 7b) and 22.3 ± 4.1 nm. This result is consistent with the absorption spectrum of the sample (Fig. 5), wherein a shoulder peak appeared at the higher wavelength side (shown by arrow) of the main SPR band. While the intense main SPR band appeared at about 536 nm corresponds to the smaller particles present in larger amount in the sample (Fig. 7b), the weaker shoulder appeared at higher wavelength side is the plasmonic contribution of larger nanoparticles (average size of 22.3 nm). However, the bimodal size distribution of nanoparticles changed to a monomodal distribution, with an average size of 22.6 ± 3.5 nm after about 60 days of preparation of the reaction solution (Fig. 7c).

The particle size distribution histograms for the 2PE, 3PE, and 5PE samples (Fig. 7d–f, respectively) studied after 10 days of their preparation revealed monomodal size distribution of nanoparticles with average diameters of 17.6 ± 3, 19.9 ± 2.4, and 21.2 ± 7.8 nm, respectively. However, the particles are more dispersed in size for the 5PE sample, because of their high nucleation rate as discussed in section 3.1.3.

To confirm the chemical nature of the nanoparticles, we performed EDS analysis (Fig. 8), and found the characteristic L (8.49, 9.70, 13.73, 13.38, 11.43 keV) and M (2.22 keV) emission lines of gold. The emissions of copper (0.95, 8.04, 8.90 keV) and carbon (0.27 keV) revealed in the EDS spectrum appeared from the used carbon-coated Cu microgrid.

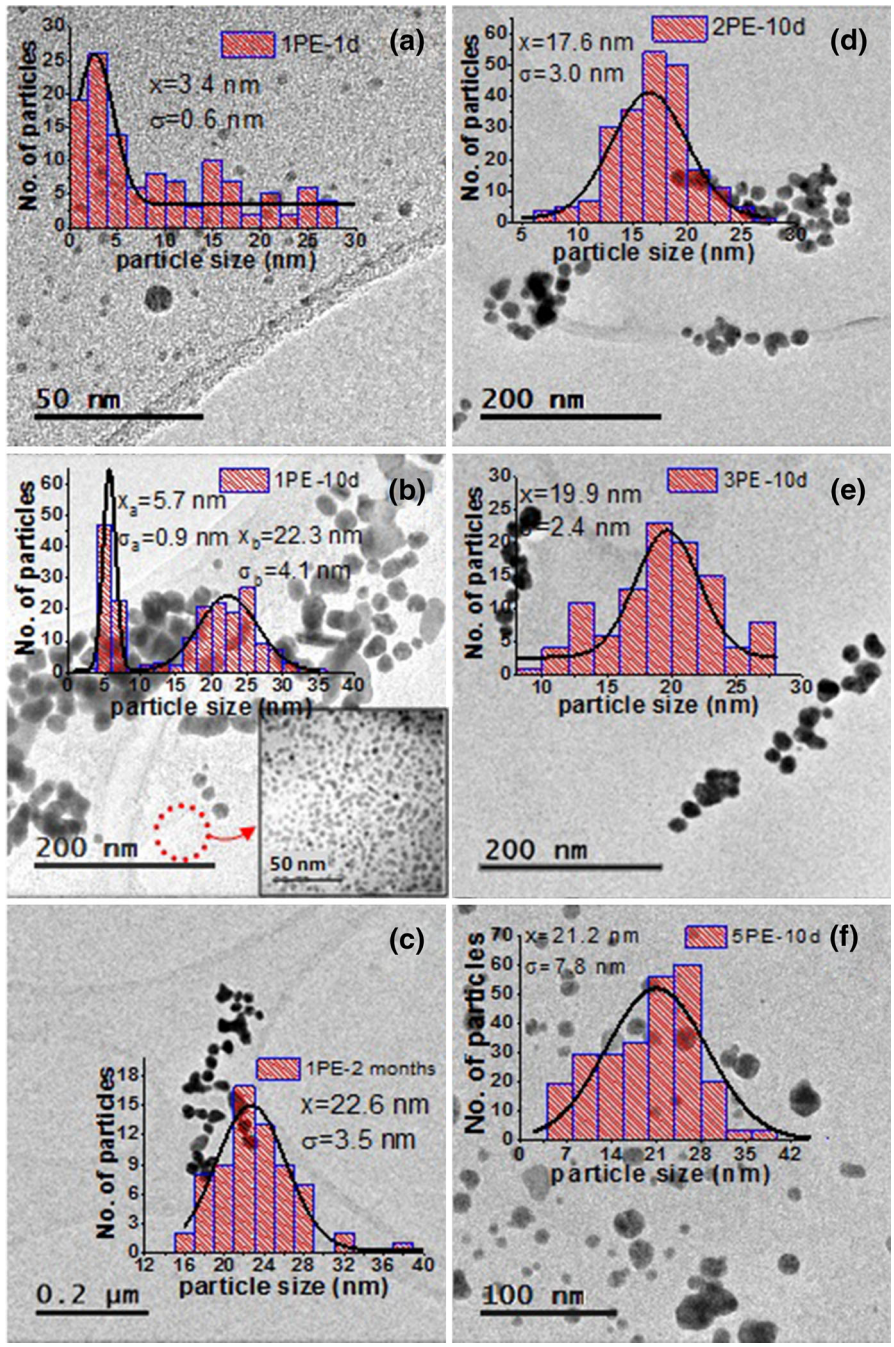

Fig. 7 Typical TEM images and corresponding size distribution histograms (*insets*) of the colloidal gold samples: **a**–**c** for the sample 1PE after 1, 10, and 60 days of reaction, respectively. **d**–**f** correspond to the samples 2PE, 3PE, and 5PE, respectively, after 10 days of reaction

As can be seen from their TEM images (Fig. 7), most of the Au nanoparticles formed in the samples have quasi-spherical morphology while a few with elongated structures, especially for the samples containing lower PE contents. On the other hand, it seems that the content of PE in the reaction mixture does not affect drastically the final size of Au nanoparticles, though a small increase in average size of the particles observed for higher PE content of the reaction mixture. On aging the colloidal samples for more than 2 months, all the smaller particles got agglomerated with the bigger particles increasing their average size a little bit.

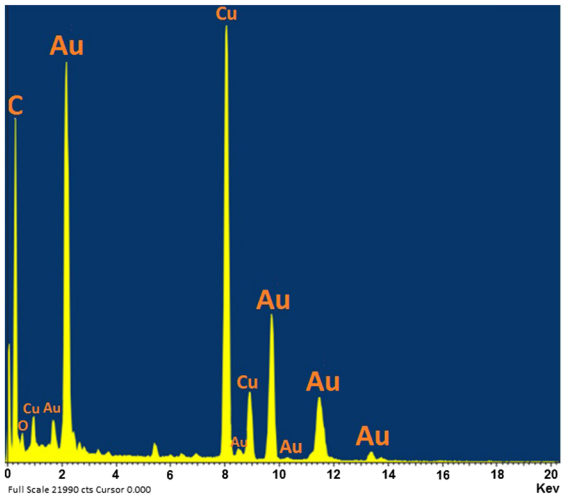

Fig. 8 EDS spectrum of the 5PE sample revealing L and M emission peaks of Au. The emission peaks associated to Cu appeared from the supporting microscopic grid

From the microscopic study of the Au NPs, the initial shift of SPR peak (blue shift) observed in the absorption spectra of the samples (Fig. 4) could be assigned mainly to the change in the refractive index of the medium (see section 3.2). After about 10 days of aging, all the smaller nanoparticles get agglomerated with the bigger nanoparticles, increasing their average size, causing a red shift of their SPR absorption peak. Such growth behaviors of the nanoparticles are expected as the used PE acts both as reducing and stabilizing agent in our synthesis process (see the stabilization mechanism section).

The high-resolution TEM (HRTEM) images and the corresponding fast Fourier transform (FFT) patterns of Au nanoparticles representative of each sample are shown in Figs. 9–12. As can be seen, all the Au particles are well crystalline, frequently with several structural/growth defects. Figure 9 shows two polyhedral Au nanoparticles of about 8 and 10 nm sizes typical to the 1PE sample. Both the particles have truncated-octahedral forms (as exemplified by the inset polyhedrons), consisting several crystalline facets with well-defined inter-planer spacing of 2.3 Å, corresponding to the (111) plane of gold in fcc phase (JCPDS # 04-0784). The FFT pattern of the first nanoparticle (Fig. 9c) shows twin defects with paired diffraction spots and reduced inter-planer spacing near grain boundaries, indicating the presence of lattice strain. The FFT pattern (Fig. 9d) of the selected area (indicated by red square in the HRTEM image) shows deformation of the diffraction spots for a particular grain associated to lattice distortion.

The second particle (Fig. 9b) presents multiple twins forming octahedral edges and stacking faults (in one of its face). The FFT pattern of the particle (Fig. 9e) clearly revealed the presence of such defects. The selected area FFT pattern of the particle revealed the stacking of (111) planes with a small lattice deformation. Most of the nanoparticles produced in sample 2EP (Fig. 10) were of icosahedral shape. The two Au nanoparticles of 17 and 15.6 nm sizes presented in Fig. 10 are typical of sample 2EP, revealing inter-planar distances of 2.3 and 2.0 Å associated to (111) and (200) planes, respectively. Since each edge of these nanoparticles corresponds to a twin defect, these particles are also recognized as a cycle penta-twined nanocrystal (Niu and Xu 2011). While the FFT pattern of 17 nm particle (Fig. 10c) revealed characteristic diffraction pattern of an icosahedral particle, the FFT pattern of its selected area (Fig. 10d) revealed the contributions of (111) and (200) planes. The 15.6 nm nanoparticle presented in Fig. 10b also revealed its icosahedral shape but it is truncated. The HRTEM image of the particle revealed the presence of (220) planes with inter-planer spacing of 1.4 Å, in addition to the planes like (111) and (200). The FFT image of the whole nanoparticle (Fig. 10e) also manifests the characteristic diffraction pattern of an icosahedral particle with twin defects and lattice deformation due to its truncated nature, while the FFT pattern of its selected area (Fig. 10f) revealed only the contribution of (111) plane.

As can be seen from Figs. 11 and 12, most of the nanoparticles formed in 3PE and 5PE samples are polycrystalline in nature, with a very few growing in single direction containing several twins and stacking faults. The polycrystalline nature of the nanoparticles is clear from their FFT patterns which are the rings consisting closely connected diffraction spots. From the analysis of HRTEM images of the Au nanoparticles formed in our samples, we can see the formation of crystalline grains with exposed faces such as (111), (200), and (200) of fcc gold lattice. As we know, the low Miller index faces such as (111), (200), and (220) are more stable than the others due to their denser

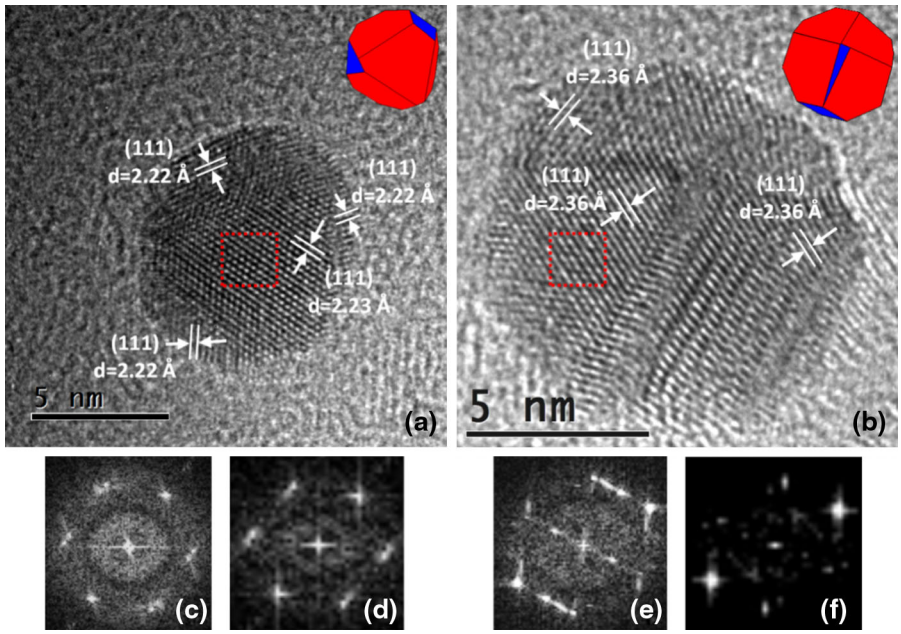

Fig. 9 HRTEM images of two typical gold particles of **a** 8, and **b** 9 nm sizes correspond to sample 1PE with truncated-octahedral shape (as exemplified in the *inset*), revealing (111) faceted planes. The FFT patterns and selected area FFT patterns of the corresponding nanoparticles are shown in (**c**, **d**) and (**e**, **f**), respectively

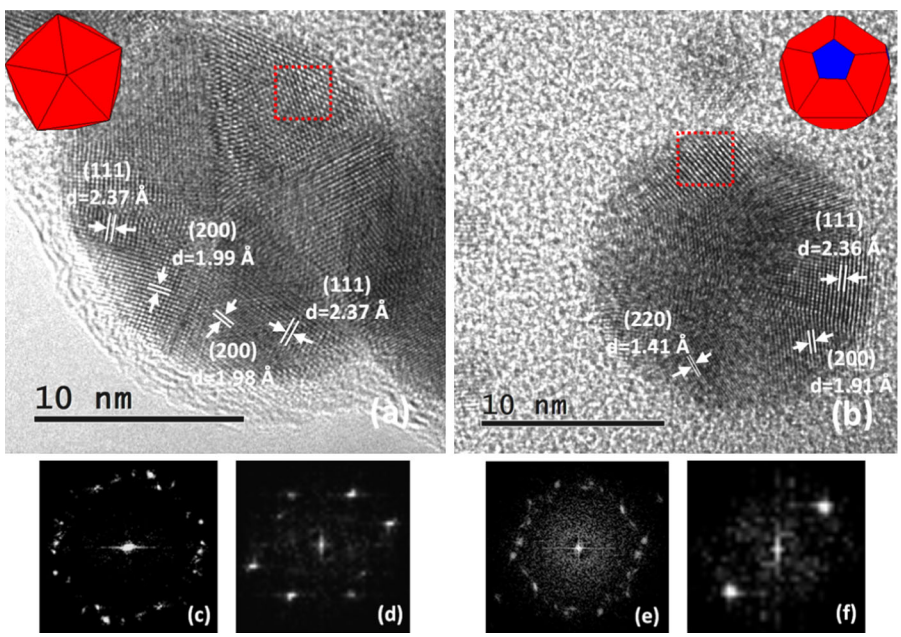

Fig. 10 HRTEM images of two typical gold nanoparticles of the 2PE sample with icosahedral shape (exemplified as *inset*) and sizes of **a** 17 nm and **b** 15.6 nm with estimated inter-planer spacing correspond to different facets. The full FFT and selected area FFT patterns of the particles shown in *left* and *right* sides are presented in (**c**, **d**) and (**e**, **f**), respectively

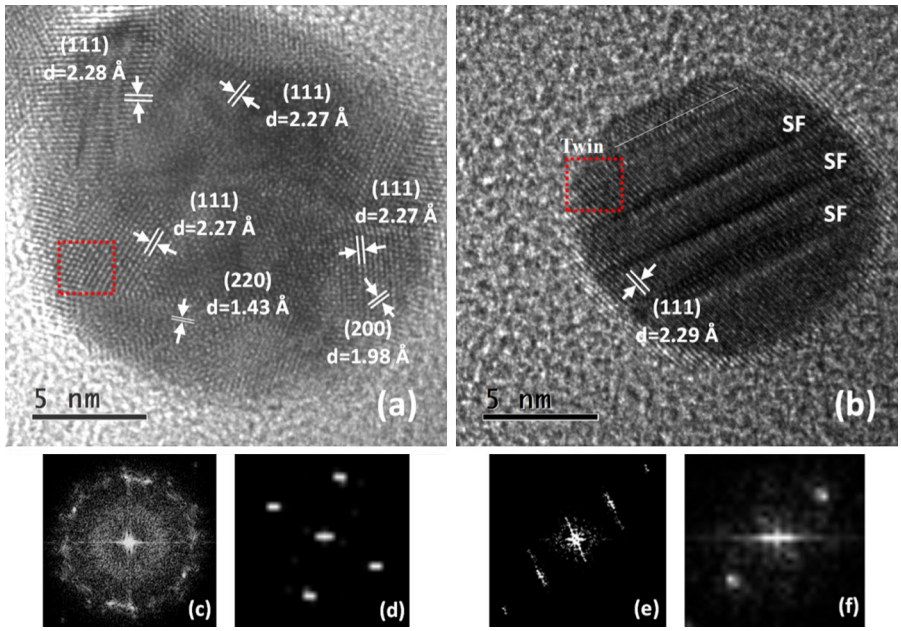

Fig. 11 HRTEM images of two typical gold nanoparticles of the 3PE sample: **a** a polycrystalline nanoparticle of 18 nm size, **b** a 13 nm crystalline nanoparticle and its (111) faceted plane showing twin and stacking faults (SF). The full FFT and selected area FFT patterns of the corresponding nanoparticles are presented in (**c**, **d**) and (**e**, **f**), respectively

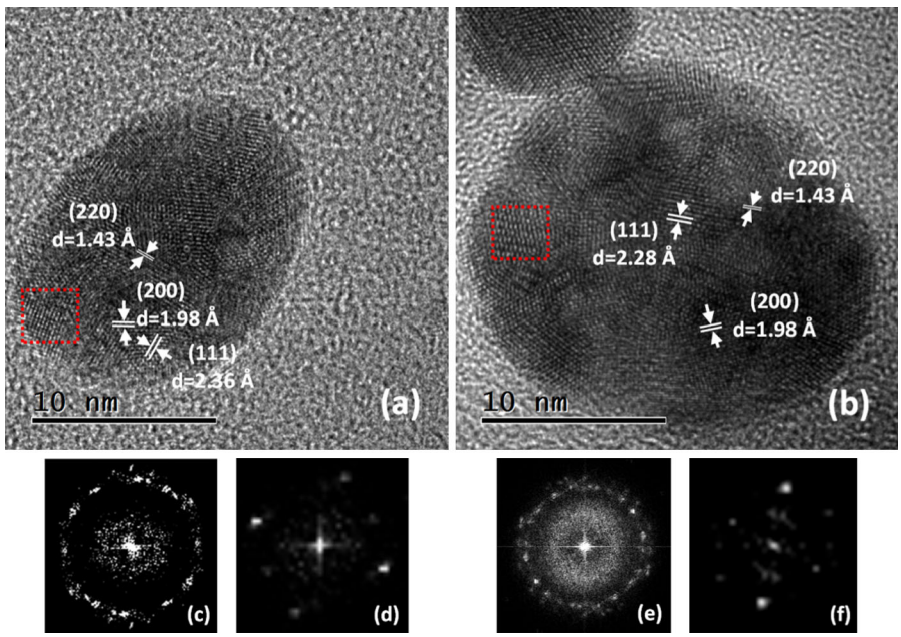

Fig. 12 HRTEM images of two typical polycrystalline gold nanoparticles of the 5PE sample of **a** 15 nm, and **b** 21 nm sizes. The full FFT and selected area FFT patterns of the corresponding nanoparticles are presented in (**c**, **d**) and (**e**, **f**), respectively

atomic packing. The presence of such denser atomic packing planes at the surface induces the formation of polyhedral structures.

In general, the 1PE and 2PE samples produced Au NPs of polyhedral shapes with well-defined facets. On the other hand, the samples 3PE and 5PE prepared

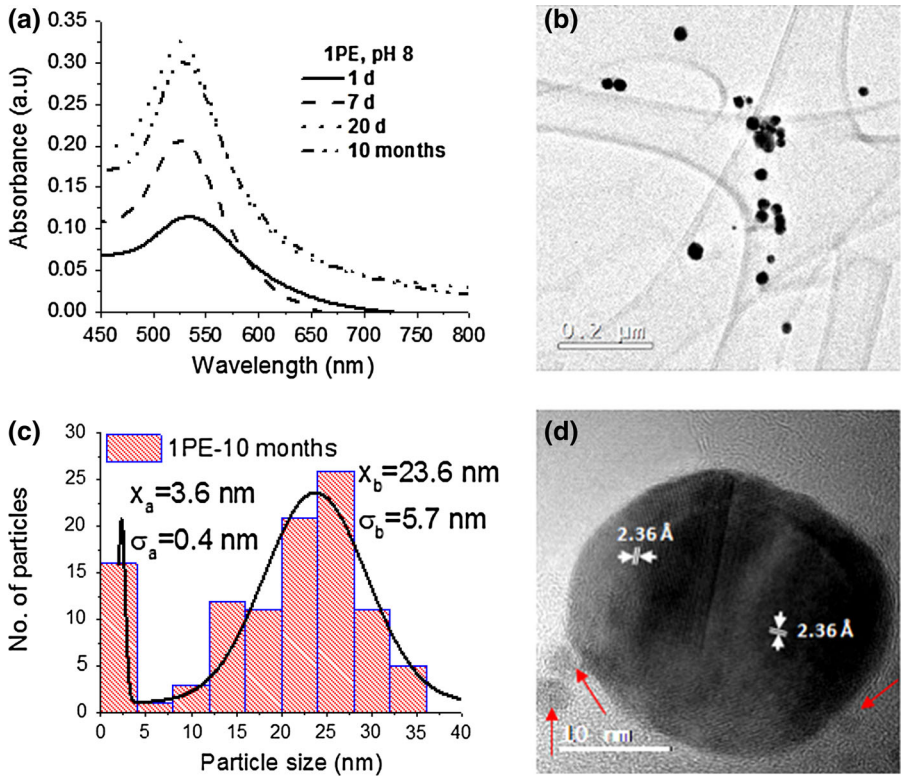

Fig. 13 **a** Absorption spectra recorded at different aging times of the 1PE sample prepared at pH 8 (alkaline medium); **b** typical TEM image, **c** size distribution histogram of Au nanoparticles, and **d** typical HRTEM image of a Au nanoparticle of 27 nm size, showing stacking faults and twining defects. The *inset* is the FFT pattern of the full HRTEM image, showing its high crystallinity and twin formation

with higher PE contents produced smaller grained polycrystalline nanoparticles of arbitrary shapes.

Reaction in alkaline medium

To study the effect of solution pH on the formation of Au nanoparticles further, we also synthesized Au NPs in an alkaline medium following the same method described above. The reaction mixture was prepared using 1 ml of potato extract ($x = 1$) and 0.5 ml of Au ion solution in 19 ml of DI water. The pH of the freshly prepared reaction mixture was adjusted to eight by dropwise addition of a standard reference buffer of pH = 10.0 (Sigma-Aldrich) under mechanical agitation. The solution was stored in the same manner as the previous samples, avoiding its exposure to light. The change in color of the solution, characteristic of the formation of colloidal Au nanoparticles, was observed after about 12 h of its preparation.

The absorption spectra of the colloidal sample recorded at different time intervals are shown in Fig. 13a. The SPR band appeared at about 535 nm after 14 h of preparation. After 20 days, the SRP peak shifted slightly toward shorter wavelengths (528 nm) due to the change in the refractive index of the reaction medium. Although the intensity of SPR band decreased slightly thereafter, its position did not change even after 6 weeks aging, and the formed NPs did not precipitate even after 10 month of sample preparation. While the above results clearly indicate a high stability of the formed Au nanoparticles, the absorption spectra of the sample always revealed well-defined SPR band with no shoulder peak, unlike the sample 1PE which was acidic in nature.

From the TEM image (Fig. 13b) and the size distribution histogram (Fig. 13c) of the nanoparticles imaged after 10 months of preparation of the sample, we can clearly note the formation of two groups of NPs (bimodal size distribution), with average sizes of 3.6 ± 0.4 and 23.6 ± 5.7 nm. We can recall that this sample was also prepared without agitation of the reaction mixture. The absorption spectrum (Fig. 13a) of the colloidal sample did not reveal any shoulder or secondary SPR band corresponding to the first group of nanoparticles, possibly due to their relatively smaller concentration. As has been presented earlier, the 1PE sample (acidic in nature) revealed a bimodal size distribution of Au nanoparticles, which gradually

changed to monomodal one after 2 months of aging due to the aggregation of smaller NPs with the bigger ones, indicating their instability in acidic solution. On the other hand, the similar sample (the present sample) prepared in alkaline solution retained its bimodal characteristic even after 10 months due to its good stability, which we discussed further in the next subsection. Further, on aging the sample until 10 months, the shape of the nanoparticles did not change (no elongated structures were formed), indicating the absence of aggregation of smaller NPs. From the HRTEM analysis of the nanoparticles (Fig. 13d), it could be noted that in general, the nanoparticles formed in alkaline medium are highly crystalline, with fewer grains and lower structural defects. While the presence of smaller NPs in the sample could be noticed (indicated by arrows) from its HRTEM image (Fig. 13d), the FFT pattern of the bigger particle revealed the formation of a well-crystalline twin with sharp and fine diffraction spots.

PE as stabilizing agent for Au NPs

As has been shown in previous sections, the colloidal Au particles synthesized in basic reaction medium are more stable than the nanoparticles synthesized in acidic media. The high stability of the former nanoparticles can be understood if we carefully analyze the effects of solution pH on the chemical stability of polysaccharides present in the reaction mixture.

As has been discussed earlier, the stability of colloidal NPs in our samples is controlled by two mechanisms: through the electrostatic interaction between the positively charged surface of metallic NPs and the (OH^-) groups of the glucose and polysaccharides present in the reaction solution, and through the steric interaction of polysaccharides wrapped over the formed nanoparticles. On changing the nature of the reaction solution from acidic to basic, though the interaction of the former type become weaker, the basic nature of the reaction mixture prevents the breaking of glucose chains strongly. While the latter action generates reducing agent in lower concentration than in acidic media, the presence of longer polysaccharide bonds creates higher steric effect, protecting the formed metallic NPs strongly against their aggregation or agglomeration, by forming denser layers around them (see Fig. 4).

As can be seen from Fig. 13c and d, the smaller Au nanoparticles formed in basic reaction medium do not agglomerated even after 10 month of sample preparation. The polysaccharide chains in the basic reaction solution are much longer than in acidic solution due to the hindering of their hydrolysis following the reaction scheme presented in Fig. 2.

In addition, due to a lower concentration of reducing agent present in the basic reaction medium, the reduction rate of the Au ions was slow (the nucleation rate was low), and hence a smaller number of Au nanoparticles were formed. Therefore, the longer polysaccharide chains could form thicker layers around them, increasing the steric effect between the neighboring particles.

Conclusions

Colloidal gold nanoparticles of 17.5–23.5 nm average sizes could be synthesized successfully in water using potato extract both as reducing and stabilizing agent. While the aldehyde groups of the D-glucose units and the reducing ends of polysaccharide chains are responsible for the reduction of gold ions, oxidized aldehyde groups of gluconic acid units and the hydroxyl groups of the polysaccharide chains are responsible for stabilizing gold nanoparticles. The aggregation of the formed nanoparticles can be controlled exploiting the steric interaction between the polysaccharide chains adsorbed on NP surface. While the amount of PE in the reaction mixture determines its final pH and hence the rate of metal ion reduction and the final size of Au nanoparticles, the pH of the reaction mixture is the main factor which determines the stability of the colloidal solution. The gold nanoparticles prepared in acidic media are stable up to about 2.5 months, in contrast with the gold nanoparticles prepared in alkaline medium, which are stable even after a year. The high stability of the colloidal particles prepared in alkaline medium is due to the presence of longer polysaccharide chains around them, which increases the steric effect of the polymer and reduces the aggregation probability of neighboring particles. Although the amount of PE in the reaction mixture has no strong effect on the final size of the nanoparticles, it affects strongly the stability of the colloidal particles and their growth behaviors. A higher PE content in the reaction mixture has seen to

produce smaller grained polycrystalline nanoparticles in larger numbers. We believe, the ambient friendly, cheap synthesis method we presented here would be very much useful not only for the controlled production of noble metal nanoparticles, the use of natural reducing and stabilizing agent like potato extract would also make these nanoparticles biocompatible.

Acknowledgments The authors are grateful to the Electron Nanoscopy Laboratory, CINVESTAV, Mexico, for extending TEM facilities used for analyzing Au nanoparticles. The work has been partially supported by VIEP-BUAP (Grant # VIEP/EXC/2014) and CONACyT, Mexico (Grant # CB-2010/151767).

References

Alschinger M, Maniak M, Stietz F, Vartanyan T, Träger F (2003) Application of metal nanoparticles in confocal laser scanning microscopy: improved resolution by optical field enhancement. J Appl Phys B 76:771–774

Armendariz V, Gardea-Torresdey JL, Yacaman MJ, Gonzalez J, Herrera I, and Parsons JG (2002) Gold nanoparticle formation by oat and wheat biomasses. In: Proceedings—waste research technology conference, Kansas city

Benet WE, Lewis GS, Yang LZ, Hughes DEP (2011) The mechanism of the reaction of the Tollens reagent. J Chem Res 35:675–677

Bo H, Shang-Bing W, Kan W, Meng Z, Shu-Hong Y (2008) Microwave-assisted rapid facile "green" synthesis of uniform silver nanoparticles: self-assembly into multilayered films and their optical properties. J Phys Chem C 112:11169–11174

Courrol LC, Silva FRO, Gomes L (2007) A simple method to synthesize silver nano-particles by photo-reduction. Colloids Surf A 305:54–57

Daniel MC, Astruc D (2004) Gold nanoparticles: assembly, supramolecular chemistry, quantum-size-related properties, and applications toward biology, catalysis, and nanotechnology. Chem Rev 104:293–346

De M, Ghosh PS, Rotello VM (2008) Applications of nanoparticles in biology. Adv Mater 20:4225–4241

Durán N, Marcato PD, De Souza GIH, Alves OL, Esposito E (2007) Antibacterial effect of silver nanoparticles produced by fungal process on textile fabrics and their effluent treatment. J Biomed Nanotechnol 3:203–208

Engelbrekt C, Sørensen KH, Zhang J, Welinder AC, Jensen PS, Ulstrup J (2004) Green synthesis of gold nanoparticles with starch–glucose and application in bioelectro-chemistry. J Colloid Interface Sci 275:496–502

Eustis S, El-Sayed MA (2006) Why gold nanoparticles are more precious than pretty gold: noble metal surface plasmon resonance and its enhancement of the radiative and nonradiative properties of nanocrystals of different shapes. Chem Soc Rev 35:209–217

Gardea-Torresdey JL, Parsons JG, Gomez E, Peralta-Videa J, Troiani HE, Santiago P, Yacaman MJ (2002) Formation and growth of Au nanoparticles inside live alfalfa plants. Nano Lett 2:397–401

Ghosh SK, Pal T (2007) Interparticle coupling effect on the surface plasmon resonance of gold nanoparticles: from theory to applications. Chem Rev 107:4797–4862

Haruta M (1997) Size- and support-dependency in the catalysis of gold. Catal Today 36:153–166

Herbani Y, Nakamura T, Sato S (2010) Femtosecond laser-induced formation of gold-rich nanoalloys from the aqueous mixture of gold-silver ions. J Nanomater 2010:1–9

Huang X, Jain PK, El-Sayed IH, El-Sayed MA (2007) Gold nanoparticles: interesting optical properties and recent applications in cancer diagnostics and therapy. Nanomed 2:681–693

Hussain ST, Iqbal M, Mazhar M (2009) Size control synthesis of starch capped-gold nanoparticles. J Nanopart Res 11:1383–1391

Iskandar F (2009) Nanoparticle processing for optical applications: a review. Adv Powder Technol 20:283–292

Jain PK, Lee KS, El-Sayed IH, El-Sayed MA (2006) Calculated absorption and scattering properties of gold nanoparticles of different size, shape, and composition: applications in biological imaging and biomedicine. J Phys Chem B 110:7238–7248

Kardos N, Luche JL (2001) Sonochemistry of carbohydrate compounds. Carbohydr Res 332:115–131

Kelly KL, Coronado E, Zhao LL, Schatz GC (2003) The optical properties of metal nanoparticles: the influence of size, shape and dielectric environment. J Phys Chem B 107:668–677

Kupiainen L (2012) Dilute acid catalyzed hydrolysis of cellulose-extension to formic acid. Dissertation, University of Oulu.

Lewis LN (1993) Chemical catalysis by colloids and clusters. Chem Rev 93:2693–2730

Liu J, Qin G, Raveendran P, Ikushima Y (2006) Facile "green" synthesis, characterization, and catalytic function of β-D-Glucose-stabilized Au nanocrystals. Chem Eur J 12:2131–2138

Liu X, Yu L, Xie F, Li M, Chen L, Li X (2010) Kinetics and mechanism of thermal decomposition of corn starches with different amylose/amylopectin ratios. Starch/Stârke 62:139–146

Maheswari RU, Prabha AL, Nandagopalan V, Anburaja V (2012) Green synthesis of silver nanoparticles by using rhizome extract of dioscorea oppositifolia L., and their anti-microbial activity against human pathogens. J Pharm Biol Sci 1:38–42

Maurer-Jones MA, Gunsolus IL, Murphy CJ, Haynes CL (2013) Toxicity of engineered nanoparticles in the environment. Anal Chem 85:3036–3049

Mock JJ, Smith DR, Schultz S (2003) Local refractive index dependence of plasmon resonance spectra from individual nano-particles. Nano Lett 3:485–491

Niu W, Xu G (2011) Crystallographic control of noble metal nanocrystals. Nano Today 6:265–285

Parida UK, Bindhani BK, Nayak P (2011) Green synthesis and characterization of gold nanoparticles using onion (Allium cepa) extract. World J Nano Sci Eng 1:93–98

Raveendran P, Fu J, Wallen SL (2003) Completely "green" synthesis and stabilization of metal nanoparticles. J Am Chem Soc 125:13940–13941

Ricard D, Roussignol Ph, Chr Flytzanis (1985) Surface-mediated enhancement of optical phase conjugation in metal colloids. Opt Lett 10:511–513

Salata OV (2004) Applications of nanoparticles in biology and medicine. J Nanobiotechnol 2:1–6

Schmid G (1992) Large clusters and colloids. Chem Rev 92:1709–1727

Shankar SS, Rai A, Ahmad A, Sastry M (2004) Rapid synthesis of Au, Ag, and bimetallic Au core–Ag shell nanoparticles using neem (Azadirachta indica) leaf broth. J Colloid Interface Sci 275:496–502

Silva-de-Hoyos LE, Sánchez-Mendieta V, Rico-Moctezuma A, Vilchis-Nestor AR (2012) Silver nanoparticles biosynthesized using opuntia ficus aqueous extract. Superficies y Vacio 25:31–35

Singh C, Sharma V, Naik PK, Khandelwal V, Singh H (2011) A green biogenic approach for synthesis of gold and silver nanoparticles using zingiber officinale. Dig J Nano Mater Biostruct 6:535–542

Sperling RA, Parak WJ (2010) Surface modification, functionalization and bioconjugation of colloidal inorganic nanoparticles. Phil Trans R Soc A 368:1333–1383

Sriburi P, Hill SE (2000) Extrusion of cassava starch with either variations in ascorbic acid concentration or pH. Int J Food Sci Technol 35:141–154

Sui Y, Cui Y, Nie Y, Xia GM, Sun GX, Han JT (2012) Surface modification of magnetite nanoparticles using gluconic acid and their application in immobilized lipase. Colloids Surf B 93:24–28

Thakkar KN, Mhatre SS, Parikh RY (2010) Biological synthesis of metallic nanoparticles. Nanomedicine 6:257–262

Vilchis-Nestor AR, Sánchez-Mendieta V, Camacho-López MA, Gómez-Espinosa RM, Camacho-López MA, Arenas-Alatorre JA (2008) Solventless synthesis and optical properties of Au and Ag nanoparticles using camellia sinensis extract. Mater Lett 62:3103–3105

Zijlstra P, Orrit M (2011) Single metal nanoparticles: optical detection, spectroscopy and applications. Rep Prog Phys 74:1–56